# Sulfur: not a "silent" element any more†

**Farideh Jalilehvand**

*Received 14th March 2006*
*First published as an Advance Article on the web 13th June 2006*
**DOI: 10.1039/b417595f**

To understand the many important functions of sulfur, a ubiquitous element in biological systems, in the environment and for industrial applications, detailed analyses are needed. Characterization of the variety of sulfur functional groups in a natural sample, often occurring in a wide range of oxidation states, became possible when the development of dedicated X-ray absorption near-edge structure (XANES) spectroscopy started in the mid-1980s. This *tutorial review* provides an overview of sulfur XANES spectroscopic investigations into the role of sulfur in all kinds of natural samples, from sediment and oil to marine-archaeological wood and plants.

## 1 Introduction

Sulfur is an element of particular environmental and biochemical importance; it is essential for plants and animals with vital functions in proteins and enzymes. Formation of sulfide minerals and of reduced sulfur compounds in coal and oil are important pathways in the natural sulfur cycle, in which human impact causes environmental concern. Fossil fuels and mining of sulfide minerals release atmospheric sour gas sulfur pollutants and acidify natural waters. Sulfuric acid is produced in larger quantities than any other base chemical, and sulfur compounds are used in numerous industrial applications such as the production of rubber, cosmetics, pharmaceuticals, pesticides and fertilizers. Sulfur is ubiquitous with a large variety of species and valence states, from −II in sulfides to +VI in sulfates. Clearly, sensitive analytical methods are needed to analyze and monitor the many functions and transformations of sulfur species in biochemical reactions and in our environment.

The predominant sulfur isotope, $^{32}S$, lacks nuclear spin and is thus not useful for nuclear magnetic resonance (NMR) spectroscopy. The $^{33}S$ isotope, with 0.76% natural abundance, has spin $I = ⅜$, providing weak and broad signals except in coordination environments of high symmetry, as *e.g.* for tetrahedral sulfate ions, sulfones, sulfonic acids and octahedral $SF_6$ molecules.[1] For sulfur species with low symmetry, such as sulfoxides, thiols and sulfides, the signals are difficult to observe with conventional instruments. However, modern high power, high field NMR spectrometers show some promise for $^{33}S$ NMR studies with its wide chemical shift range of more than 1000 ppm.[1,2]

Because of the lack of informative and specific analytical methods, sulfur has been called a spectroscopically "silent element". While the total sulfur concentration can be easily determined, the characterization of sulfur species in a mixture represents a real challenge. The recent development in synchrotron-based X-ray absorption near-edge structure (XANES) spectroscopy, is therefore of particular interest. This new possibility to identify and determine different types of sulfur species in a natural sample opens up new fields of opportunities for understanding their chemical reactions and for controlling their effect and influence on the environment and in life sciences.

*Department of Chemistry, University of Calgary, 2500 University Dr. NW, Calgary, Alberta, Canada T2N 1N4.*
*E-mail: faridehj@ucalgary.ca; Fax: +1(403) 289-9488*
† The HTML version of this article has been enhanced with colour images.

**Farideh Jalilehvand**

*Farideh Jalilehvand has been Assistant Professor in Physical Inorganic Chemistry at the University of Calgary, Canada, since July 2002. After her MSc in 1993 from Sharif University of Technology (Tehran, Iran), she achieved her first PhD in synthetic inorganic chemistry at the Ochanomizu University (Tokyo, Japan) in 1997. She continued her studies at the Royal Institute of Technology (KTH) (Stockholm, Sweden), applying synchrotron-based X-ray absorption spectroscopy on metal complexes in solution, and achieved her second PhD in inorganic chemistry in 2000. She was then employed as a Research Associate at the Stanford Synchrotron Radiation Laboratory (California, USA), where she could apply sulfur XANES spectroscopy to marine-archaeological samples from the 17th century Swedish warship Vasa. The discovery of sulfur accumulation in historical shipwrecks was published in Nature and received worldwide attention. She currently holds a University Faculty Award from the Natural Sciences and Engineering Research Council of Canada (NSERC).*

## 2 Theory

The X-ray radiation from a synchrotron source is very intense with a continuously variable, wide range of energies, from low energies spanning from about a few hundred eV up to more than a hundred keV. A sample exposed to X-rays absorbs part of the radiation and the intensity $I_0(E)$ of the incident beam with energy $E$, is reduced to $I(E)$ according to Beer's law in the form:

$$\log[I_0(E)/I(E)] = (\mu(E)/\rho)x \quad (1)$$

 

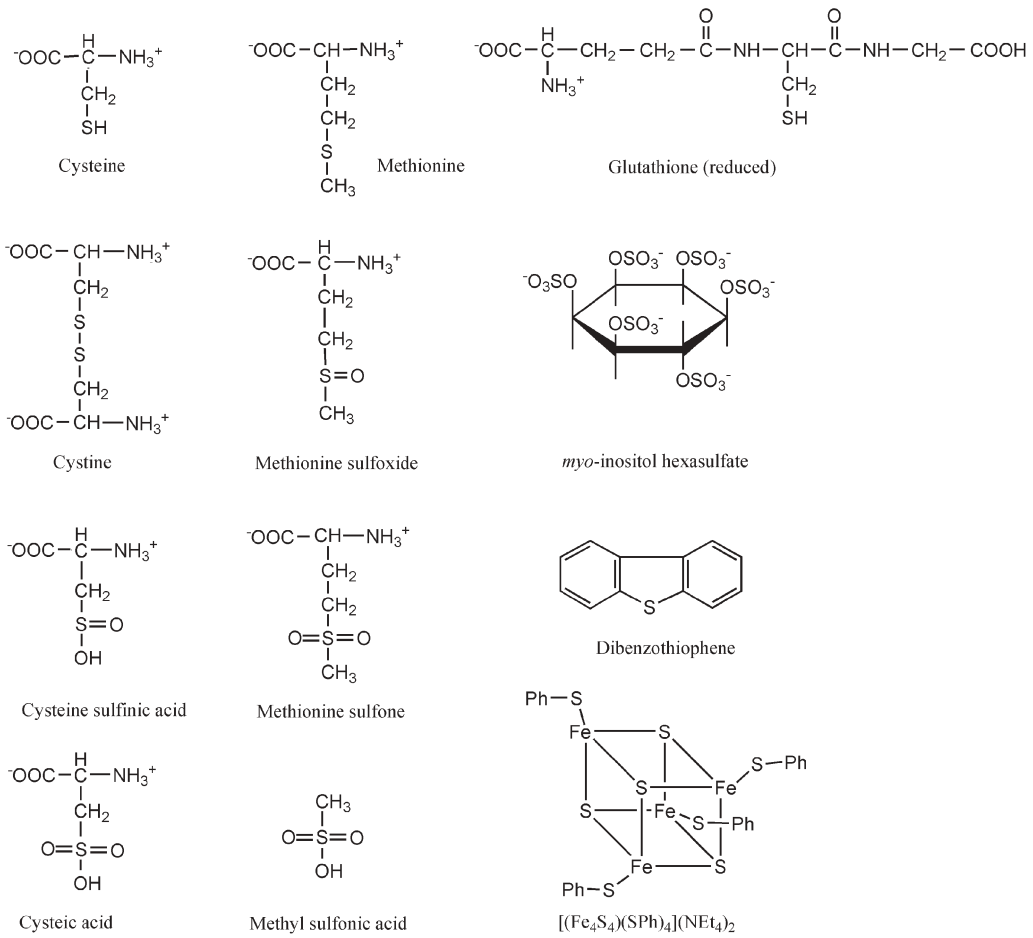


**Scheme 1** Structural formulae for some model compounds for characteristic sulfur groups with their normalized (standard) spectra shown in Fig. 1 and 2.

where $\mu(E)$ is the linear absorption coefficient ($cm^{-1}$), $\rho$ the density (g $cm^{-3}$), and $x$ ($=\rho t$) the mass thickness (g $cm^{-2}$) of the sample with thickness $t$ (cm). The mass absorption coefficient ($\mu/\rho$ in $cm^2$ $g^{-1}$) of the sample can be obtained from tabulated mass absorption coefficients $(\mu/\rho)_i$ as:

$$(\mu/\rho)_{\text{sample}} = \Sigma w_i(\mu/\rho)_i \qquad (2)$$

where $w_i$ is the mass fraction of the element $i$.[3]

The penetration depth of the X-rays into the sample, $\sin\theta/\mu(E)$, depends on the incident X-ray angle $\theta$ and is inversely related to the linear absorption coefficient $\mu(E)$ of the material.[4] The absorption generally decreases with increasing X-ray energy, however, sudden increases, known as absorption edges, occur when the X-ray energy is sufficient to overcome the binding energy of a core electron in an element $i$. The absorption edges for sulfur occur at 2472 eV (K), 230.9 eV ($L_1$), 163.6 eV ($L_2$) and 162.5 eV ($L_3$), and correspond to the creation of a photoelectron from the 1s, 2s, $2p_{½}$ and $2p_{⅔}$ core levels, respectively.[5] A higher formal oxidation state of the sulfur atom will reduce the shielding of the nuclear charge and raise the binding energy of the core orbitals. Thus, the energies of the sulfur absorption edges are sensitive to the sulfur oxidation state (*cf*. Fig. 1 and 2). At the K-edge there is a large shift of about 13 eV from sulfides (−II) to sulfate (VI).[6]

An X-ray absorption spectrum can be considered in four energy regions.[7] The lowest energy part, the pre-edge region (*i*), is followed by the region of the sharply rising absorption edge (*ii*). In these two regions the incident photon energy is below the ionization threshold and the distinct absorption peaks that occur correspond to electronic transitions to an unoccupied bound state valence level. The edge inflection point can be used to estimate approximately the core binding energy $E_0$. Not only the position of an edge but also the shape and position of the peaks in the pre-edge region depend on the oxidation state, the geometry of the coordination sphere and the character of the bonding between the neighboring atoms and the absorbing element. By analysing the edge and the pre-edge features, information about the electronic structure and the surrounding of the photo-absorbing atom can be obtained. In the near edge region (*iii*), loosely defined as the range between the absorption edge up to ~40 eV above the edge, the incident X-ray energy $E$ is higher than that of the absorption edge $E_0$, and the excited electron leaves the absorbing atom as a photoelectron with relatively low kinetic energy: $E_K = E - E_0$. Multiple-scattering of the photoelectron then occurs within the first and second shell of the surrounding atoms and the absorption spectrum may display a complex structure known as "shape resonances". The XANES spectral region of interest for analytical

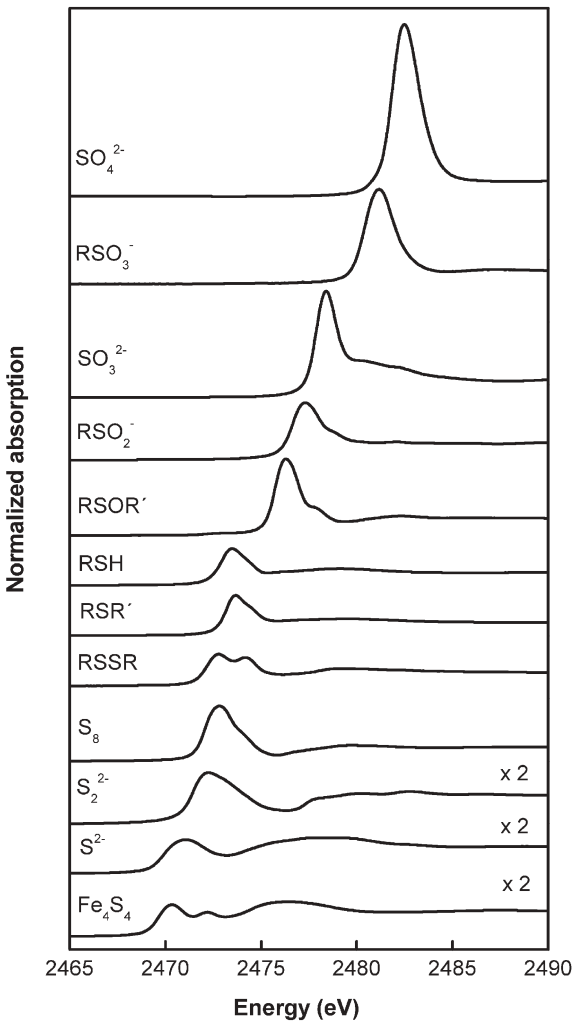


**Fig. 1** Normalized sulfur K-edge XANES spectra measured in fluorescence mode of the $[(Fe_4S_4)(SPh)_4](NEt_4)_2$ cluster (containing $\mu_3$-sulfide and aromatic thiolate), solid iron sulfide FeS (with $S^{2-}$) and pyrite $FeS_2$ (with $S_2^{2-}$), a solution of elemental sulfur ($S_8$) in *p*-xylene, aqueous solutions (pH = 7) of L-cysteine (RSH), L-cystine (RSSR), L-methionine (RSR′) and methionine sulfoxide (RSOR′), solid L-cysteine sulfinic acid ($RSO_2^-$), aqueous solutions of sodium sulfite $Na_2SO_3$ ($SO_3^{2-}$) at pH = 10.6, mesylic acid $CH_3SO_3H$ ($RSO_3^-$) at pH = 1.8 and sodium sulfate ($SO_4^{2-}$) at pH = 6.3.

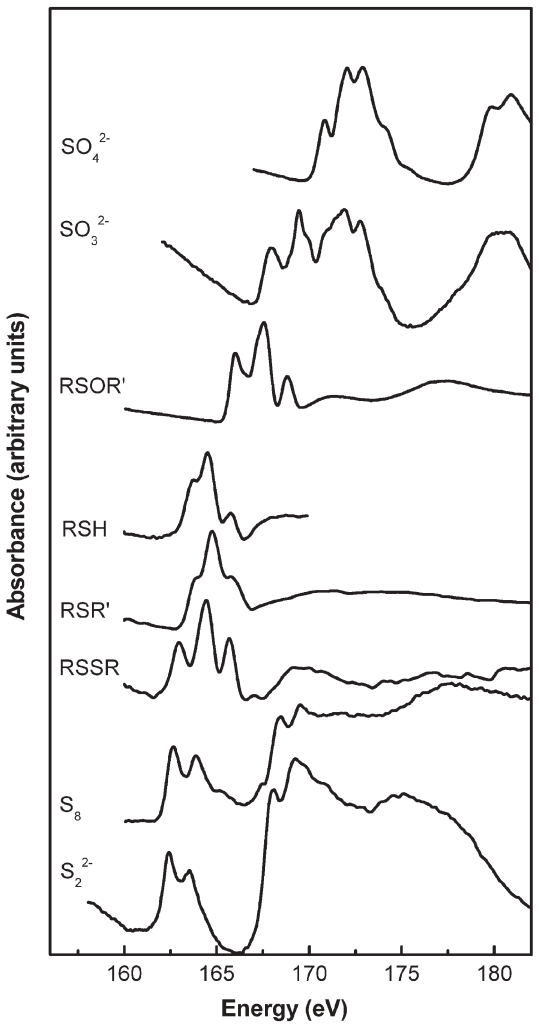


**Fig. 2** Sulfur L-edge XANES spectra measured with total electron yield of solid model standards: pyrite ($S_2^{2-}$), elemental sulfur ($S_8$), DL-cysteine (RSH), DL-cystine (RSSR), DL-methionine (RSR′), DL-methionine sulfoxide (RSOR′), sodium sulfite ($SO_3^{2-}$) and sodium sulfate ($SO_4^{2-}$) (ref. 14, 21).

purposes is normally the region within about $\pm 10$ eV around the edge.

The oscillatory part of an X-ray absorption spectrum, which occurs at X-ray energies $\sim$40–1000 eV above the edge, is known as the extended X-ray absorption fine structure (EXAFS) region (*iv*). The photoelectron then obtains high kinetic energy and single back-scattering from the nearest neighbour atoms dominates, providing information about their number and identity and also the distance from the absorbing atom.[7,8]

At the sulfur K-edge there are intense pre-edge features corresponding to dipole allowed transitions that involve excitation of an 1s electron to antibonding molecular orbitals, which are formed with significant contribution from the sulfur p-orbitals and are localized around the sulfur atom.[9] With increasing formal oxidation state of the sulfur atom the energy of the s level decreases more than that of the p level (lower energy level = increasing binding energy). The energy of the transition with 1s $\rightarrow$ 3p character then increases and shifts the edge and the pre-edge peak positions to higher energies.[10] Also the intensity of the spectral features increases. For the sulfur K-edge the probability of the transition largely depends on the contribution of the sulfur p orbital to the valence molecular orbital.[11] The reduced shielding of the nuclear charge at higher oxidation state contracts the 3p and 1s orbitals. The consequently increased orbital overlap, and the stronger transition dipole arising from polar bonding, cause sulfates to exhibit a spectral intensity several times higher than that of sulfides (*cf*. Fig. 1).

The geometry and covalency of the bonds also influence the unoccupied valence molecular orbitals around the sulfur atom (see below) and contribute to the transition energies and intensities. Therefore, in the sulfur K-edge XANES spectrum, the transition energies and the shape of the absorption features contain specific information about the character of the bonds formed to the sulfur atom.[11,12]

 

Correlating the oxidation state to the XANES peak position is useful when characterizing different types of sulfur functional groups. For a series of compounds, Frank *et al.* empirically found that the absorption maxima in the K-edge XANES spectra varied almost linearly with the oxidation state of the sulfur atom. The energy of maximum absorption increased by 1.6 ± 0.2 eV over a total range of 13 eV per unit change from 0 to +6 of the formal oxidation state.[12] Vairavamurthy observed that virtually identical K-edge XANES spectra were obtained, independent of the organic side chains, for various organosulfur compounds with the same sulfur functional group, *i.e.* with similar local surrounding of the sulfur atom.[13] To experimentally rank the oxidation states of sulfur in different types of complex molecules, he correlated the apparent oxidation state to the energy of the characteristic peak positions in a scale with fix-points, assigning the formal oxidation state 0 to elemental sulfur (at 2473.1 eV) and +6 to sulfate (at 2483.1 eV; note the different energy calibration schemes described in Section 3 below). Vairavamurthy found that the values for the oxidation state derived from the XANES data in this way generally were inconsistent with the formal values. He therefore defined an "oxidation index" for different types of sulfur functional groups as: di- and polysulfides, +0.2 (2473.3 eV), thioethers and thiols +0.6 (2474.1 eV), thiophenes +1.0 (2474.7 eV), sulfonium compounds +1.9 (2476.2 eV), sulfoxides +2.2 (2476.8 eV), sulfones +4.3 (2480.4 eV), sulfonates +5.2 (2481.7 eV) and ester sulfates +6.1 (2483.2 eV). This scale reflects that the sulfur K-edge XANES peak positions are not only indicative of the oxidation state, but also influenced by the local bonding environment.[13]

Sulfur L-edge XANES spectroscopy has been used less frequently than the K-edge, partly because the high air absorption of soft X-rays makes vacuum conditions necessary.[4] Sulfur $L_{2,3}$-edge transitions, which occur in the 160–190 eV region, start at the 2p level and, according to the angular momentum selection rules, end at final states with mainly d or s character. Therefore, the $L_{2,3}$-edge spectra probe the sulfur d-orbital contributions to the molecular orbitals, which are sensitive to the more distant environment around the sulfur atom. The L-edge spectra always contain several peaks due to the spin–orbit splitting of the p-level and also display higher resolution.[14] For example, in the sulfur $L_{2,3}$-edge spectrum of the $SF_6$ molecule the peaks have been attributed to the promotion of a sulfur 2p electron to unoccupied molecular orbitals of $a_{1g}$, $t_{2g}$ and $e_g$ symmetries with the first two absorption peaks split into doublets due to the spin–orbit coupling of the 2p core electrons into $2p_{1/2}$ and $2p_{3/2}$ states.[15]

There are several factors affecting the experimental energy resolution, including *e.g.* the core hole lifetime, the excited electron life-time, instrumental broadening mainly due to imperfections and mosaic structure of the monochromator crystals, and for solid samples self-absorption effects (see below). Yu *et al.* experimentally determined the energy resolution at the beamline 6-2 at the Stanford Synchrotron Radiation Laboratory (SSRL), to 0.51 eV from the width of the peak at 2471.4 eV for the single transition ($1s \rightarrow \pi^*(3b_1)$) in $SO_2$(g).[16] For sulfur, the natural width $\Gamma$ of the core level (related to the core hole lifetime by the uncertainty relation: $\tau_h\Gamma \approx 6.6 \times 10^{-16}$ eV s) is ~0.4 eV for the K-level and ~0.1 eV for the $L_3$-level.[4] Hence, the longer core hole lifetime $\tau_h$ is the main reason for the higher resolution and sharper peaks at the sulfur L-edge.

The higher resolution and the increased sensitivity to the more distant valence shell orbitals at the $L_{2,3}$-edge facilitate discrimination between different reduced sulfur functional groups with significant overlap in their K-edge XANES spectra. Fig. 2 presents the S $L_{2,3}$-edge spectra for some pure compounds, for which the S K-edges are shown in Fig. 1. For most reduced sulfur species, the L-edge spectra show three peaks in the 162–168 eV region, each arising from several electronic transitions. The transition energy increases with increasing formal oxidation state of the sulfur atom, from disulfides (R–S–S–R′), to alkyl sulfides (R–S–R′), aryl sulfides (Ar–S–Ar), dibenzothiophene and thiophene (not shown here). For the oxidized sulfur species, the broad features in the 166 to 183 eV region of the S $L_{2,3}$-edge spectra make it difficult to discriminate between sulfonate and sulfate in a complex mixture. Therefore, to identify reduced sulfur groups, $L_{2,3}$-edge XANES spectra are useful, but less so for oxidized species and for quantitative analyses.[14] In contrast, sulfur K-edge spectra often allow fairly precise determination of the relative amounts of the characteristic sulfur groups, with the highest accuracy for the oxidized sulfur species.[14]

## 3 Experiment

Beamlines allowing measurements at the X-ray energies required for the sulfur absorption edges are available at many synchrotron facilities. The X-rays, enhanced by an insertion device in the storage ring, are often diffracted from a double Si(111) crystal monochromator.[6,13] Efficient elimination of harmonics‡ is important, especially in the soft X-ray regime, as the intensity of the fundamental can be lower than that of X-rays with higher energy passing the monochromator due to the energy profile of the synchrotron radiation. For sulfur K-edge measurements, the use of a fully tuned crystal monochromator followed by removal of higher harmonics by means of metal (Ni, Pt or Rh) coated mirrors reduces the intensity less than "detuning", which is performed by misaligning the 2nd monochromator crystal relative to the first one. For efficient monochromatization with detuning, only ~20–30% of the incident intensity of the X-ray beam should be retained at the sulfur K-edge.[10,17,18]

Data collection by scanning over an absorption edge with fine monochromator steps (<0.1 eV) takes usually a few minutes. The intensity of the incident X-rays can be monitored by means of a helium-filled ion chamber. Sample preparation is normally easy, and sulfur K-edge XANES spectra can even be measured on intact samples in atmospheric pressure of helium, which is useful *e.g.* for environmental investigations.[6] Note that most tapes and films contain appreciable amounts of

‡ X-Rays are reflected in a set of two coplanar monochromator crystals according to the Bragg law: $n\lambda_d = 2d\sin\theta$, with the spacing $d$ between the planes in the crystal, $n = 1$ represents the fundamental with wavelength $\lambda$ and $n > 1$ the "harmonics", with wavelength $\lambda_d/n$.

sulfur compounds and must be tested for sulfur content if used as a window material in the beam path or for sample holders.

Careful energy calibration is necessary to allow comparisons between XANES spectra from model compounds and samples. Determinations of the absolute energies have not been sufficiently accurate so far, and several schemes and standards are in use to obtain precise relative energies for repeated measurements. Vairavamurthy added NaCl to the samples, and calibrated the sulfate peak to 2483.1 eV using the chloride edge as internal standard. The first peak position of sodium thiosulfate, $Na_2S_2O_3 \cdot 5H_2O$, then appeared at 2472.4 eV, and elemental sulfur at 2473.1 eV.[13] Sekiyama *et al.* calibrated the energy of the first intense peak in the sulfur K-edge absorption spectrum of NiS powder to 2469.8 eV, which placed the first peak for $Na_2S_2O_3 \cdot 5H_2O$ at 2469.2 eV and sulfate at 2479.9 eV.[19] Williams *et al.* assigned the maximum of the first pre-edge feature in the sulfur K-edge spectrum of $Na_2S_2O_3 \cdot 5H_2O$ to 2472.02 eV.[20] Kasrai *et al.* used elemental sulfur for calibration, assigning its strong peak (white line) at the K-edge to 2472.0 eV and the lowest energy peak at the $L_{2,3}$-edge to 162.7 eV.[21] Hence, when comparing spectra from samples measured by different groups the calibration scheme that was used must be identified. In the current review the energies of the peaks are given as reported in the corresponding reference articles.

The number of incident X-ray photons absorbed by the atoms in the sample is proportional to the number of created core holes.[4] The electron structure of the atom can adjust by the transition of an electron from a higher energy level to the vacant hole. The energy difference is released in two competing processes, either as fluorescence radiation or by emission of Auger electrons. The relative rates are described by the Auger yield $\omega_a$ and the fluorescence yield $\omega_f$, respectively, with $\omega_a + \omega_f = 1$ and with the Auger process favored for low $Z$ atoms.[4,22] For the core holes in the L and K shells of sulfur, the fluorescence and Auger yields are 0.03% and 99.97%, and 8% and 92%, respectively.[21,22]

Three types of detection modes are in use for measuring sulfur K- and L-edges: total electron yield (TEY), Auger electron yield (AEY) and fluorescence yield (FY), while transmission measurements, which are often used at higher energies, would require extremely thin samples at the sulfur K-edge energy. Since the escape depth of the electrons is quite small,[4] Auger electron detection provides surface information, while X-ray fluorescence measurements can probe deeper into the bulk of the sample. Total electron yield measures the entire range of electrons emitted from the sample with a sampling depth typically about $\sim$5 nm for the S $L_{2,3}$-edge compared to about 70 nm for the K-edge.[14,23] For the sulfur K-edge fluorescence detection has been used mostly, while for the L-edge electron yield detection is preferred because of the low fluorescence yield.[21]

Pickering *et al.* pointed out that self-absorption attenuates the peaks measured in fluorescence mode when the X-ray absorption coefficient changes significantly within the energy range of the spectrum.[24] Thus, XANES spectra obtained from concentrated or thick samples (*e.g.* solid model compounds) may become distorted. For solids careful grinding and dilution (*e.g.* with boron nitride or graphite) reduce self-absorption, but if the sulfur concentration is high the required particle size becomes too small to be achieved by grinding (*e.g.* $<1$ μm for elemental sulfur[25]). In such cases total electron yield detection can be less sensitive to attenuation effects since the incident X-rays penetrate much deeper than the escape depth of the emitted electrons, and the contributing volume would vary less. Charging of the sample that may distort the spectra should be minimized by diluting with a small quantity of conductive graphite.

Beside the self-absorption effects, there are other differences between the XANES spectra of sulfur compounds in solids and solutions (Fig. 3). The long range order in the solid state induces multiple-scattering effects which, together with multi-electron excitation processes, contribute to the features on the high energy side of the absorption edge. Hence, when analysing solutions or dilute amorphous samples, standard spectra of solid model compounds are often less suitable for modelling the experimental spectra (see below).

## 4 Data analysis

The data treatment techniques are under rapid development, both theoretical simulations of spectra allowing in depth studies of the bonding and electronic structure, and practical data handling for deconvolution and speciation when analyzing complex systems. The sulfur XANES spectra from natural samples often contain overlapping features from several transitions. For analytical purposes, deconvolution of the peaks and separation of the components are often necessary for achieving chemical speciation and reliable evaluation of the relative amounts of the characteristic sulfur groups. In a series of spectra, the number of components can be obtained by means of principal component analysis. The identification of the components requires a library of normalized spectra collected from model compounds with the characteristic sulfur

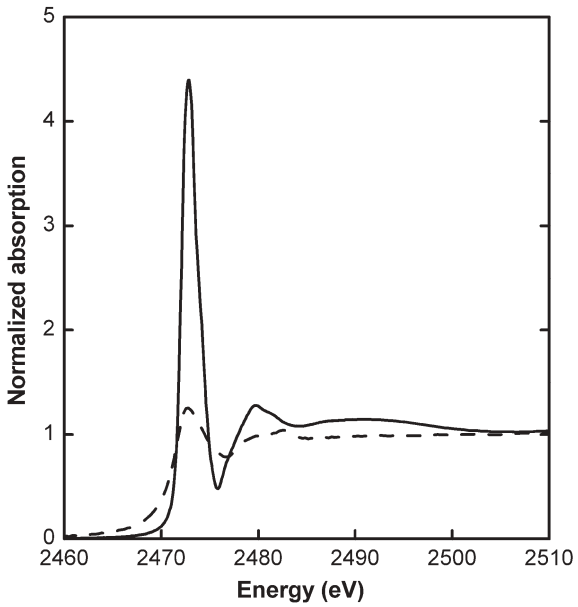


**Fig. 3** Normalized sulfur K-edge XANES spectra measured in fluorescence mode of elemental sulfur ($S_8$) in *p*-xylene solution (—) and as a thin film of finely ground powder (---).

 

group in a similar local surrounding and bonding condition as in the sample. Curve-fitting with a linear combination of these normalized standard spectra to that of the sample can reveal the composition and relative amounts of the sulfur functional groups in the sample.

An example using DATFIT in the EXAFSPAK suite of computer programs[26] is shown for magnolia leaves in Fig. 4. The components are selected considering possible functional groups in the sulfur metabolism and sulfate assimilation processes in higher plants. For instance, cysteine ($H_2Cys$; component 1) residues are common building blocks in proteins and in peptides such as glutathione. Methionine (component 2) is the other essential sulfur-containing amino acid, which can be produced by plants, bacteria, yeasts, *etc*., but not in the human body, and can be found in cheese, fish, meat and vegetables. Even though the S K-edge XANES spectra of the model components 1 and 2 are quite similar[24] (Fig. 4, see also Section 5.2 below), in this case the fit improved significantly when both components were included. One approach utilized to check whether appropriate components were chosen for the model spectrum is to compare its 2nd derivative with that of the experimental spectrum (with high signal-to-noise). In addition, measurements at the sulfur L-edge can provide additional information.

At the sulfur K-edge, the absorption intensities of oxidized sulfur species, such as sulfate at about 2482 eV, are about three times greater than those of the more reduced forms near 2473 eV. This difference allows relatively higher precision when analyzing species that contain trace amounts of high oxidation state components. The overall error in the reported percentages of the components in a fit, such as the one shown in Fig. 4, generally corresponds to the statistical uncertainties determined by the noise level in the data, also small differences in normalization or calibration among standard spectra and between data sets, and the ambiguity arising from generally unknown structural and environmental differences between the compounds used as models and the compounds in a given sample (see below). One should thus report the individual statistical uncertainties calculated by the algorithm for each of the model components used in the fit. In EXAFSPAK, the calculated statistical uncertainties are included in the output list file.

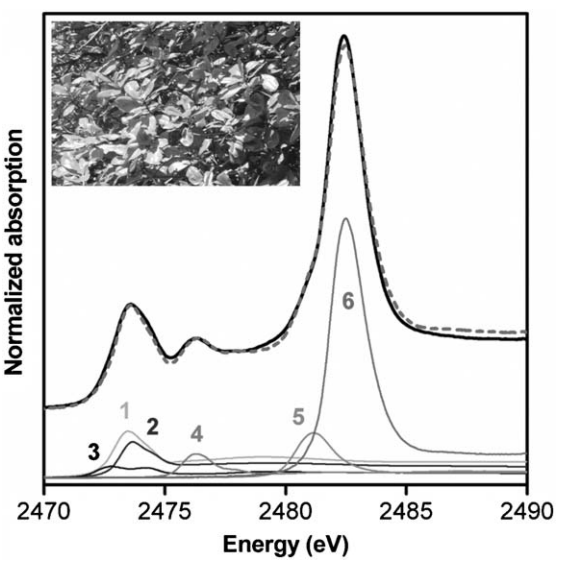


**Fig. 4** (*top*) Sulfur K-edge XANES spectrum of a magnolia leaf (—), the model (---) with (*below*) the corresponding components: thiol (1, 24%), thioether (2, 17%), disulfides (3, 7%), sulfoxide (4, 6%), sulfonate (5, 9%) and sulfate (6, 37%). The relative amounts are in atom% S (ref. 36).

A complete approach to fit error also requires estimating the overall structural uncertainties in the final fit by evaluating how different models that give similar fits affect the percentage of each component. This can be achieved, *e.g*., by evaluating the effect of adding or removing one member of the set of components, or by interchanging model compounds with similar functional groups (*e.g*. different thiol-containing species). In this light, the overall estimated error for the reported percentages in Fig. 4 is about 10% of the relative amount found by the fit, *i.e*., for the components 1 + 2 that are estimated to comprise 41 atom% of the total amount of S, the error is within $\pm$ 4 atom% S, and for the sulfonate (component 5) with an estimated amount of 9 atom% S, the error is about $\pm$ 1 atom% S.

It is essential for curve-fitting purposes that the model compounds are in an appropriate condition. The absorption peaks in the S K-edge XANES spectra of compounds in natural samples are often affected by factors such as the pH of the medium, possible complex formation with metal ions present in the sample, or slight distortions in the molecular symmetry in solution or in the solid state.

For example, the S K-edge XANES spectrum of methionine shows little sensitivity to variations in the pH in aqueous solution, while for cysteine a drastic change occurs when changing the pH from 7 to 13 (*cf*. Fig. 5). With increasing pH the major peak loses intensity and shifts toward a lower energy, because the shielding of the sulfur orbitals increases when the thiol (–SH) group of the cysteine molecule deprotonates.[24]

Complex formation with transition metal ions with vacant d-orbitals can give rise to new spectral features. For the cysteine complexes of $Ni^{2+}$ ($d^8$), $Mo^{5+}$ ($d^1$) and $Cr^{3+}$ ($d^3$) with different binding modes to the cysteine ligand, a distinct pre-edge peak appears at about 2472 eV, which is not present for similar complexes of $Hg^{2+}$ and $Cd^{2+}$ with $d^{10}$ configuration (*cf*. Fig. 5 and 6).[27] Such pre-edge features have been discussed in depth by Solomon *et al*. and assigned as S 1s transitions to antibonding molecular orbitals with both metal d- and sulfur 3p-character (see also Section 5.1 below).[11,20,28] The intensity depends on the number of vacancies in the d-orbitals of the transition metal ion, and the covalency of the metal–thiolate bonding. In some cases this pre-edge feature overlaps with an S 1s $\rightarrow$ ligand C–S $\sigma^*$ transition, which occurs at energies below the rising edge of the transition with 1s $\rightarrow$ 4p character (see Section 5.1).

Reduced symmetry may also affect the spectral features. An example is the tetrahedral ($T_d$) sulfate ion, $SO_4^{2-}$, for which the S 1s $\rightarrow$ (valence $t_2$) transition is observed at 2482.4 eV (thiosulfate calibration 2472.02 eV, see above). When it is protonated to $HSO_4^-$, or binds as a monodentate ligand to a metal ion, the point group symmetry is reduced to $C_{3v}$ and the

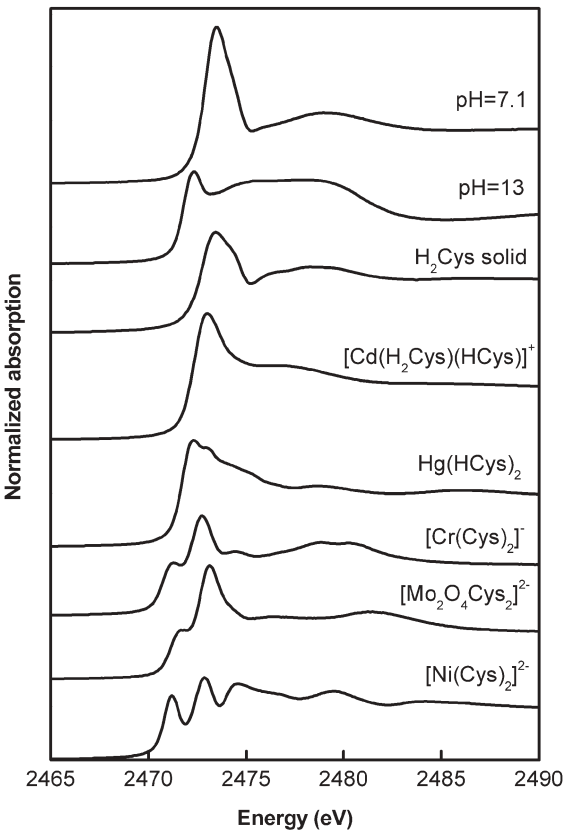


**Fig. 5** Normalized sulfur K-edge XANES spectra measured in fluorescence mode. From top: cysteine in aqueous solution at pH = 7.1 ($HCys^-$) and pH = 13 ($Cys^{2-}$), solid cysteine ($H_2Cys$), $[Cd(H_2Cys)(HCys)](ClO_4)$, $Hg(HCys)_2$, $Na[Cr(Cys)_2]$, $Na_2[(\mu\text{-}O)_2(O{=}MoCys)_2]$ and $K_2[Ni(Cys)_2]$ complexes (ref. 27).

triply degenerate $t_2$ state splits into two symmetry species, $a_1 + e$. The corresponding $1s \rightarrow a_1$ and $1s \rightarrow e$ transitions occur at slightly different energies and broaden the peak in the spectrum. The magnitude of the splitting reflects the distortion from ideal tetrahedral symmetry, and is less for the hydrogen sulfate ($HSO_4^-$) ion than for *myo*-inositol hexasulfate, which contains six covalently bonded sulfate esters (*cf.* Scheme 1, Fig. 7). The relative intensity of the transitions at 2480.8 and 2482.8 eV corresponds to the 1:2 degeneracy of the $a_1$ and e orbitals, respectively.[12] In some complexes the point group symmetry is further reduced, *e.g.* to $C_{2v}$, and the triply degenerate $t_2$ state will then resolve into its three single components and consequently broaden the absorption peak.[29]

The physical state of a model sulfur compound also affects its S K-edge XANES spectrum. Often sulfur species in dilute solution display sharper features than for solids because of self-absorption in the particles (*cf.* Fig. 3). Other factors affecting the intensity of the features are the bond covalency, the strength of hydrogen bonding, and in solution also the solvent interaction and the effect of a fluctuating dielectric field.[30]

The examples mentioned above clearly illustrate how important it is that the standard XANES spectra should be obtained from sulfur groups in a similar state and surrounding as in the sample. When deconvoluting overlapping XANES peaks, even small shifts in the energy calibration or in the

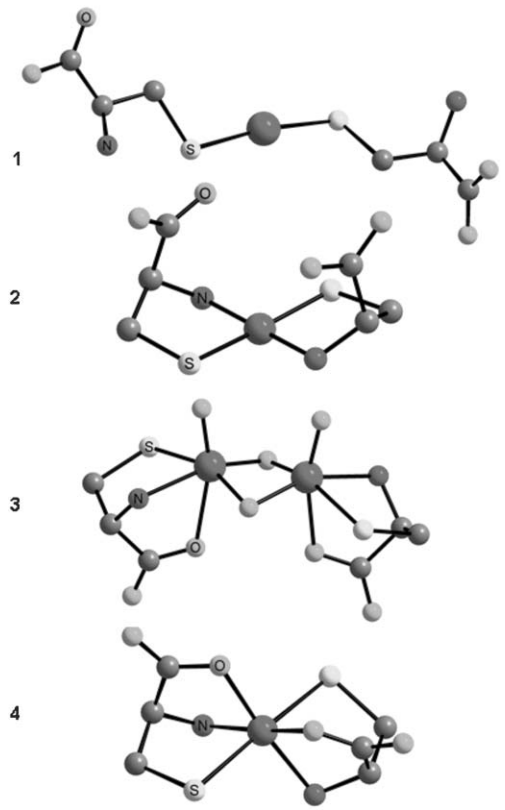


**Fig. 6** Structure of the complexes of cysteine ($H_2Cys$) in $Hg^{II}(HCys)_2$ (1), $K_2[Ni^{II}(Cys)_2]$ (2), $Na_2[(\mu\text{-}O)_2(O{=}Mo^{V}Cys)_2]$ (3) and $Na[Cr^{III}(Cys)_2]$ (4).

transition energies or intensities due to chemical interactions, will increase the uncertainty of the analysis. Moreover, note that evaluating *e.g.* disulfides in a biological sample with a

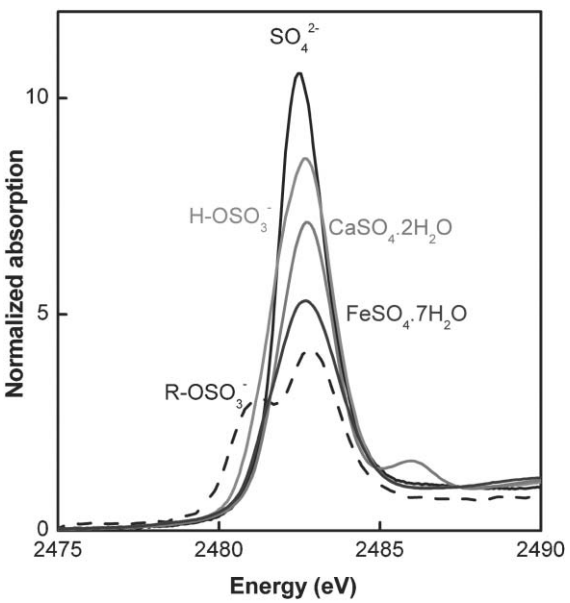


**Fig. 7** Sulfur K-edge XANES spectra of: $SO_4^{2-}$ (pH = 6.3), $HSO_4^-$ (pH = 0), the solids gypsum $CaSO_4{\cdot}2H_2O$ (note the characteristic feature at 2486 eV), melanterite $FeSO_4{\cdot}7H_2O$, and *myo*-inositol hexasulfate R-$OSO_3^-$ (ref. 12).

 

model compound such as cystine provides a sum of all disulfides, including *e.g.* both oxidized glutathione and protein disulfides.[24]

## 5 Applications

XANES spectroscopy provides a sensitive probe for chemical speciation of sulfur with many applications in biological systems, such as the mechanisms for detoxification and heavy metal regulation in living organisms, and sulfur metabolism in bacteria and plants including characteristic sulfur compounds in mushrooms and vegetables. The sulfur cycle in nature is heavily affected by human impact and many aspects with environmental importance are poorly understood. Examples will be given below of the occurrence and origin of sulfur species in heavy oils and asphaltenes, in humic substances, in soil and marine sediments. Also, sulfur XANES spectroscopy has helped to understand why acidity can develop in marine-archaeological wood, which is a concern for the conservation of historical shipwrecks.

### 5.1 Structure and bonding in coordination compounds

Sulfur K-edge XANES is used as a powerful experimental method to probe the covalency of thiolate–metal bonds, *e.g.* in $M(SR)_4^{2-}$ complexes, where M = Cu(II), Ni(II), Co(II), Fe(II), Mn(II) and R = (2-Ph–$C_6H_4$).[11] In S-thiolate ligands, one of the 3p valence orbitals of sulfur contributes to the strong S–C bond. Another of the two remaining sulfur p orbitals is used for a pseudo σ-bond and the third for a π-bond to the metal ion.[28] Because the 1s → *n*p transitions are electric dipole allowed for K-edges, the intensity of the pre-edge feature provides a direct probe of the metal–S bonding interactions. As an example, a well-defined pre-edge peak appears when a thiolate is bound to a $d^9$ Cu(II) ion, corresponding to the ligand 1s → ψ* transition, where ψ* is the half-filled molecular orbital with a contribution from Cu $3d_{x^2-y^2}$. Due to the covalency in the Cu–S bond the molecular orbital also obtains a significant component of sulfur 3p character that confers absorption intensity to the transition:

$$\psi^* = (1 - \alpha^2)^{1/2}[\text{Cu } 3d_{x^2-y^2}] - \alpha[\text{S(ligand)3p}] \qquad (3)$$

where $\alpha^2$ measures the amount of sulfur 3p character contributing to the molecular orbital ψ*.[20]

Also for other $d^n$ metal centers with more than one hole in the d-manifold, pre-edge features are observed that correspond to several transitions from the sulfur 1s orbital to unoccupied antibonding molecular orbitals with contributions both from metal d- and sulfur p-orbitals.[20] In the S K-edge spectra of $M(SR)_4^{2-}$ complexes, an additional peak may appear, which has been assigned as the S 1s → ligand C–S σ* transition, at energies below the rising edge of the main sulfur 1s → 4p transition. In some cases these two pre-edge features are not resolved.[11]

Similar methodology has been used to determine the covalency of the Cu–S bond in the mononuclear blue Cu site, *e.g.* in plastocyanin, and the binuclear $Cu_A$ sites *e.g.* in cytochrome *c* oxidase and nitrous oxide reductase. Also, the Fe–S bonds in the redox-catalysing rubredoxin and ferredoxin iron–sulfur clusters have been studied to obtain insight in the biological functions of electron transfer proteins.[11] For example, quantitative analysis of the pre-edge intensity in the S K-edge spectrum of the blue Cu site in plastocyanin shows as much as 38% sulfur 3p character in the highest singly occupied molecular orbital. The high covalency implied in the Cu(II)–S(Cys) bond can be connected to the rapid, long-range electron transfer process.[28]

Significant changes of transition energies may also appear in the sulfur XANES spectra of metal complexes with a sulfur-containing ligand, when the covalency of the bonding changes. We recently compared the sulfur K-edge XANES spectra for several dimethyl sulfoxide solvated group 13 metal ions, Al(III), Ga(III), In(III) and Tl(III), all with six octahedrally oxygen-coordinated dimethyl sulfoxide ligands, and noticed a splitting of the main absorption feature with a different intensity distribution than that for the uncoordinated dimethyl sulfoxide molecule. XANES spectra were simulated by means of Kohn–Sham density functional theory (DFT) calculations to interpret these features. It was concluded that the M–O bonding affects the orbital interactions in the dimethyl sulfoxide S=O bond with partial double bond character and enhances the splitting of the transitions. The largest effect occurs for the Tl(III) solvate with the most covalent M–O bonding.[31]

### 5.2 Chemical speciation of sulfur in biological systems

Cysteine and methionine are the sulfur-containing amino acids found in all cells. Methionine, R–S–$CH_3$, can reversibly be oxidized to its sulfoxide, R–S(O)–$CH_3$ and, also, further to the sulfone, R–$S(O)_2$–$CH_3$. For cysteine (or cysteine residues in proteins) two thiol groups can reversibly connect to form a disulfide bridge as in cystine (*cf.* Scheme 1). This bridge formation, which is important *e.g.* for protein folding, changes the biological functions of proteins and peptides, *e.g.* their enzymatic properties. Sulfur XANES spectroscopy is an analytical tool that can measure the thiol–disulfide ratio, which seems to serve as a metabolic signal.[32] Rompel *et al.* used the characteristic differences between the thiol and disulfide groups in sulfur K-edge XANES spectra (see Fig. 1) to determine the redox status in biological systems, such as intact cells, whole human blood, plasma and red blood cells (erythrocytes) with a sensitivity of ~5% in the thiol-to-disulfide ratio. The spectra were measured in the fluorescence mode at 140 K to reduce radiation damage. The sulfur XANES spectrum of red blood cells was very similar to that of reduced glutathione (GSH), indicating that thiol groups are dominating in the sulfur species. In blood plasma, the model fit with GSH and the oxidized disulfide GSSG as model compounds, resulted in 32% thiol and 68% disulfide groups, while whole blood was found to contain 54% thiol and 46% disulfide.[32]

Also Pickering *et al.* have reported sulfur speciation in biological systems, carefully considering the possible experimental pitfalls that were mentioned earlier.[24] They found that even for two compounds as similar as cysteine and methionine, noticeable differences could be detected in their S XANES spectra. Deconvolution revealed at least two transitions in the

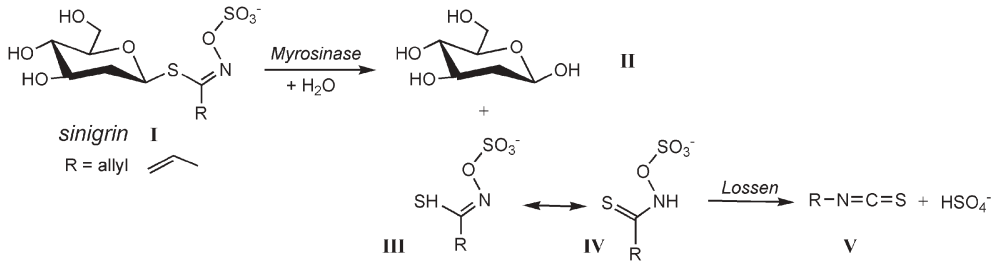


**Fig. 8** Hydrolysis of sinigrin in horseradish and wasabi produces isothiocyanate and sulfate through a Lossen rearrangement (ref. 16).

major peak of these compounds, which are expected to be 1s $\rightarrow \sigma^*$(S–C) and possibly 1s $\rightarrow \pi^*(CH_2)$. These two features have the same separation (0.88 $\pm$ 0.03 eV) and intensity ratio (0.43 $\pm$ 0.10) in cysteine and methionine, but are shifted to 0.2 eV lower energy for cysteine. The intensities of the edge features of methionine and cysteine were found to be similar, although very slightly ($\sim$2.5%) higher for methionine. They also discussed for cysteine and reduced glutathione GSH that, even though the major peaks are virtually identical, there are some differences in the multiple scattering region above the edge. The disulfides cystine and oxidized glutathione show two clearly resolved peaks, separated by about 1.5 eV, which have been assigned as 1s $\rightarrow \sigma^*$(S–S) and 1s $\rightarrow \sigma^*$(S–C) transitions, for the lower and higher energy peaks, respectively.[24] For curve-fitting analyses of the sulfur XANES spectra of the red blood cells (erythrocytes) and plasma from horse blood, Pickering *et al.* for aliphatic disulfides, thiols, thioethers and sulfoxides used as model oxidized glutathione, cysteine, methionine and methionine sulfoxide, respectively, and also sulfate. All model compounds were in aqueous solution at pH 7. The best fit for the erythrocytes indicated 21.4% disulfide, 54.4% thiol, 21.3% thioether, 2.1% sulfoxide and 0.8% sulfate, whereas the best fit for the plasma yielded 76.5% disulfide, 20.6% thiol, 0% thioether, 0% sulfoxide and 2.9% sulfate with an estimated accuracy within $\pm$5% of the reported values.[24]

Frank *et al.* used vanadium and sulfur K-edge XANES to investigate the distribution of sulfur species in whole blood cells and in plasma samples from the tunicate *Ascidia ceratodes*.[12] The average vanadium(III) concentration in such blood cells is about 1–2 million times higher than that in ambient seawater. The concentration of sulfur in the blood cell of this organism has been found to be 0.25 M, which is about 9 times higher than the normal concentration in biological systems. The sulfur K-edge XANES spectrum of a sample of whole blood cells showed two major peaks, one for low-valent sulfur near 2473–2474 eV and another, more intense peak for oxidized sulfur near 2482 eV. The second derivative of the peak at 2473–2474 eV revealed a doublet, probably from endogenous disulfides. Two principal features were distinguished for the oxidized sulfur at 2481.1 and 2482.4 eV, corresponding to sulfonates and sulfate ions with the oxidation states +5 and +6, respectively. By precipitating and removing sulfate as $BaSO_4$, the presence of sulfonate, evidently complexed by vanadium(III) ions in the lysate, could be confirmed.[12]

Sulfur K-edge XANES has been used to identify and quantify the chemical forms of sulfur in the cells of a variety of sulfide-oxidizing bacteria, including photosynthetic sulfur bacteria, which metabolize sulfur compounds and store "sulfur globules". Previously, it was proposed that such globules, which can become quite large (up to 1 μm in diameter) and are hydrophilic with relatively low apparent densities, could contain elemental sulfur in a "liquid" or amorphous form. Several hypotheses were developed to explain these anomalities.[25] A transmission sulfur K-edge XAS study by Prange *et al.* suggested that the globules contain long chains of sulfur terminated by carbon atoms.[33] However, Pickering *et al.* could, after correcting their spectra for self-absorption in the sulfur globules, conclude that the most probable major form of sulfur in the globules is simply normal elemental sulfur, $S_8$.[25]

### 5.3 Sulfur in plants

Horseradish and wasabi belong to the cruciferous family of plants, which contain large amounts of sinigrin, a glucosinolate with a bitter taste that is stored in subcellular organelles in the intact cell (Fig. 8, **I**). Upon cell damage, the odorless sinigrin is hydrolyzed by myrosinase enzyme and releases volatile compounds with intense flavor such as allyl isothiocyanate (Fig. 8, **V**). Yu *et al.* utilized sulfur K-edge XANES to identify the sulfur species in horseradish and wasabi *in situ*, both in the intact tissues and in cells damaged by bruising.[16] Fitting the XANES spectra using sinigrin, allyl isothiocyanate (R–N=C=S), methionine (R–S–$CH_3$) and sulfate as model compounds, revealed that sinigrin ($\sim$50%) and sulfate ($\sim$30%) are the two major sulfur species in the intact cells of both plants. The quantitative conversion of sinigrin to isothiocyanate and sulfate in damaged cells was monitored. A small peak at low energy (2468 eV) was attributed to an S 1s $\rightarrow$ (C=S) $\pi^*$ transition associated with C=S $\pi$-bonding, consistent with an intermediate thio-acid amide sulfate (Fig. 8, **IV**).

Sulfur-rich plants of the *Allium* family, such as garlic, onion and Chinese chive, also release strong aromas from damaged cells due to the formation of a complex mixture of sulfur species, originating from a family of odourless γ-L-glutamyl-cysteine sulfoxide precursors, during a two-step enzymatic process[34] (*cf.* Fig. 9). The precursors **1** are oxidized to L-cysteine sulfoxides **2**, which are converted to highly reactive sulfenic acid intermediates **3**, that spontaneously form the flavor-containing species (thiosulfinates, *etc.*).

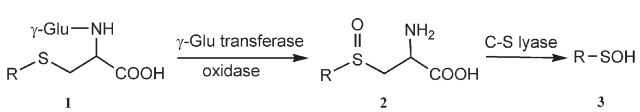


**Fig. 9** Postulated mechanism for production of sulfenic acid **3** from precursors **1** and **2** in alliums and shiitake mushrooms (ref. 34).

 

One might presume that the garlic-like odour released from shiitake mushrooms (with R = $CH_3SO_2CH_2S(O)CH_2S(O)$–, in Fig. 9) is also produced through similar biochemistry. To identify the organosulfur species in alliums and shiitake mushrooms, Sneeden *et al*. measured the S K-edge XANES spectra of intact and juiced plant tissues of onion, garlic, Chinese chive and shiitake mushroom.[34] Aqueous solutions at neutral pH of reduced and oxidized glutathione, methionine, methionine sulfoxide, methionine sulfone and sulfate were used to obtain standard spectra for speciation. In the intact tissue of all four types of samples, the sulfoxide precursor together with reduced sulfur forms including thiols, disulfides, sulfides, and a small amount of sulfate were present. For the shiitake mushroom an additional peak corresponding to sulfone groups was observed. The proportion of sulfur species in intact shiitake tissue was found to be: disulfide (R–S–S–R′) 2%, thioether (R–S–R′) 19%, sulfoxide (R–S(O)–R′) 60%, sulfone (R–$SO_2$–R′) 16%, and sulfate 3%. This 3.75:1 sulfoxide-to-sulfone ratio is similar to the 3:1 ratio of these groups in precursor **2** with R = $CH_3SO_2CH_2S(O)CH_2S(O)$–. The transformation of sulfur species occurring at the point of cell damage can be easily monitored, since for the juiced allium species the sulfoxide peak intensity decreases and those of the reduced forms of the flavorant molecules increase. However, the sulfur species in shiitake mushrooms were quite stable and no significant changes in their S K-edge XANES could be observed at cell damage, leaving the biochemistry of its flavor an enigma still.

In plants, not only the spicy aromas of horseradish, wasabi, onion, garlic or shiitake mushrooms signify the presence of sulfur! In fact, sulfur species are found in all kinds of plants, as part of the sulfur cycle in nature. The plants convert sulfate to reduced sulfur forms through a sulfate assimilation process and are important as a source of the essential amino acid, methionine.[35]

To monitor the sulfur metabolism in urban trees by identifying the sulfur functional groups of the major metabolites in intact plant leaves, six samples were collected near the Stanford University campus and the Golden Gate Park in California, US, from Southern Magnolia (*cf*. Fig. 4), Monterey Pine, Giant Sequoia, California Juniper, California Redwood and Bluegum Eucalyptus. The S K-edge XANES spectral features showed similar major sulfur species with peaks at 2473, 2476 and 2482 eV that are characteristic for thiols, sulfoxides and sulfates, respectively, merely with slightly different ratios.[36] The fitting indicated that the major chemical forms of sulfur in the leaves were thiol (–SH) and thioether groups, disulfides, sulfoxides, sulfonate (R–$SO_3^-$) and sulfates. The total amount of the reduced sulfur forms (thiol + disulfide + thioether) was typically about 44–55 atom% S, and the oxidized forms (sulfonate + sulfate) between 38–50 atom% S, and about 6–10 atom% S as sulfoxide.

### 5.4 Sulfur in archaeological samples

Sulfur spectroscopy has been used to reveal the cause of conservation concerns for famous historical shipwrecks, such as the almost intact 17th century Swedish warship *Vasa* (sank in 1628), and the flagship of Henry VIII's navy *Mary Rose* (capsized in 1545 when preparing for battle).[37,38] Sulfur K-edge XANES together with elemental sulfur analyses revealed that about 2 tons of sulfur in different reduced forms had accumulated in the timbers of both the *Vasa* and the *Mary Rose* during their time on the seabed. At the European Synchrotron Radiation Facility (ESRF) beamline ID21 scanning X-ray microspectroscopy, at resonance energies for reduced and oxidized sulfur, localized organosulfur compounds (thiols and disulfides) mainly in the lignin-rich middle lamella between the wood cells.[38,39] In addition, when iron ions from corroding iron objects were available, particles of iron(II) sulfides, *e.g*. pyrrhotite $Fe_{1-x}S$ and pyrite $FeS_2$, together with elemental sulfur, have formed in the waterlogged wood. By comparing the distributions of reduced and oxidized sulfur and iron compounds for the *Vasa* and the *Mary Rose* with that of the *Bremen Cog* (1380), which was preserved in sweet river water and therefore almost sulfur-free, the accumulation mechanisms were elucidated. Surprisingly high concentrations of reduced sulfur compounds accumulate in waterlogged wood, preserved in oxygen-depleted conditions in sulfate-containing seawater. A new pathway in the sulfur cycle was found, where bacterially-produced hydrogen sulfide reacts with lignin in the wood forming thiols in the primary step. That process resembles the anaerobic process in humic matter and marine sediment (see Section 5.5 below), where the accumulated sulfur eventually may end up as sulfur contamination in fossil fuels, in coal and oil. In the shipwrecks oxygen access to the moist marine-archaeological wood, in the presence of catalyzing iron ions, can cause severe detrimental acidity by oxidation of the reduced sulfur compounds, in the first place the iron sulfides, to sulfuric acid, as is occurring for the *Vasa*.[39]

### 5.5 Sulfur in environmental samples

Marine sediments are a source for generating petroleum and contain significant amounts of a wide variety of organosulfur compounds. In anoxic marine sediment the major organosulfur functional groups are: thiols, thioethers, disulfides, polysulfides and thiophene derivatives, some of which were also found in the core samples of historical shipwrecks preserved in anoxic environments lying on or below the seabed (see Section 5.4). Vairavamurthy and co-workers used sulfur K-edge XANES spectroscopy to explore the compositional relationships between different sulfur forms in sediments.[18] Two major absorption bands were observed in these spectra; one in the 2471–2475 eV region for the reduced sulfur compounds that included both organic species (*e.g*. thiols, thioethers, disulfides, polysulfides, thiophenes) and inorganic species (*e.g*. pyrite, iron sulfides and elemental sulfur), and the other band in the 2480–2485 eV region for oxidized sulfur species (*e.g*. sulfonates and sulfates). XANES fitting procedures revealed that 20–40% of the total organosulfur compounds near the surface (0–7 cm depth) of the marine sediment samples were in the form of sulfonates. Other major sulfur forms were pyrite, thioethers, polysulfides, and sulfate. The amount of reduced forms (mainly polysulfides/disulfides) was highest in the subsurface layers. The presence of a large variety of sulfonates in the living organisms, such as marine plants and animals, suggests

that sedimentary sulfonates may be produced through both biological and geochemical pathways.

Organic matter in soils and sediments is originally from plant and animal residues, which transform to dark brown-black humic substances through microbial and chemical processes known as humification. Vairavamurthy *et al.* investigated the sulfur composition in sedimentary humic substances by analysing sulfur K-edge XANES spectra of humic acid extracts from different near-surface marine sediments and found the major sulfur groups to be thioethers, di- and polysulfides, sulfonates (15–40%) and sulfate esters (10–25%). The organosulfur composition in humic acids is often similar to that of the source sediments, except for pyrite-containing sediments, for which the extract of humic acids did not contain pyrite. Pyrite is formed by the reaction of iron minerals with hydrogen sulfide, which is produced by anaerobic bacterial reduction of sulfate in marine sediments. No thiophenic sulfur was found in these near-surface marine sedimentary humic acids, possibly because thiophenes are usually produced in deeper layers of the sediment column.[40]

Humic substances are also thought to be the precursors of petroleum-forming kerogen and it seems that sulfur plays a key role in converting humic substances to source-rock kerogen. Removing sulfur from oil, coal and petroleum products is of great importance, to reduce the pollution originating from releasing sulfur compounds into the atmosphere through combustion processes. Such removal requires monitoring of the different sulfur compounds (organic and inorganic) that are present in coal or oil.

One early sulfur K-edge XANES and EXAFS investigation on the speciation and quantification of organosulfur compounds in a petroleum asphaltene sample showed sulfur surrounded by two carbon atoms at the average S–C distance 1.74(2) Å, suggesting that aromatic sulfur compounds similar to dibenzothiophene were present in the asphaltene sample. The sulfur composition in two other asphaltene samples, however, revealed a mixture of thiophenic and sulfidic forms, as evidenced by the appearance of sulfide peaks at 2469.8 eV in the 3rd-derivatives of the sulfur XANES spectra.[9]

Sarret *et al.* investigated sulfur species in asphaltene samples collected from archaeological and geological bitumens from the Middle East, France and Spain using sulfur XANES spectroscopy.[14] Sulfur L-edge XANES analyses showed that the major reduced sulfur species in all samples are dibenzothiophenes and the minor species in the least oxidized samples are disulfides, alkyl and aryl sulfides, and thiophenes. As the amount of these minor species decreases, sulfoxides and/or sulfones are formed. Sulfur K-edge XANES fittings of the asphaltene samples revealed the relative proportions of sulfoxides, sulfones, sulfonates and sulfates. They concluded that the contribution of sulfonates was very low, while the sulfoxide + sulfone content varied between 12–36% in the samples.

Kasrai *et al.* also characterized the sulfur species in asphaltenes and bitumens using a combination of sulfur K- and L-edge XANES spectroscopy. The spectra were collected in both TEY and fluorescence yield modes to monitor differences between the sulfur composition on the surface and the bulk of the sample. The L-edge XANES spectra of bitumens and asphaltenes were almost identical and similar to that of an alkyl substituted, thiophenic sulfur model compound. A relatively good fit was obtained by constructing a model spectrum with 70% thiophenic sulfur + 30% thianthrene. No alkyl disulfides or any significant amounts of oxidized sulfur compounds could be detected in the S K-edge spectra of these samples.[23]

Huffman *et al.* reported quantitative sulfur speciation in coal using sulfur K-edge XANES spectroscopy and concluded that the main sulfur functional groups in Argonne Premium Coal Sample Bank (APCSB) coals were pyrite, thioethers, and thiophene, with minor amounts of sulfoxide, sulfone and sulfate groups being present. However, the XANES spectra of maceral separates, which were obtained from grinding the coal to fine particles and therefore were exposed to the air, showed pronounced peaks from sulfur–oxygen bonded compounds (*i.e.* sulfones and sulfates).[10]

Information about how sulfur dissolves in silicate melts (glass) can provide better understanding of the geochemical behavior of sulfur in magmas. Under reducing conditions sulfur mainly dissolves as sulfide, and as sulfate under oxidizing conditions:

$$\tfrac{1}{2}S_2 + O^{2-} \leftrightarrow \tfrac{1}{2}O_2 + S^{2-} \quad (4)$$

$$\tfrac{1}{2}S_2 + \tfrac{3}{2}O_2 + O^{2-} \leftrightarrow {SO_4}^{2-} \quad (5)$$

The major factor controlling the relative abundance of these two species, is oxygen fugacity:

$${S^{2-}}_{melt} + 2{O_2}_{\ gas} \leftrightarrow {{SO_4}^{2-}}_{melt} \quad (6)$$

Paris *et al.* used sulfur K-edge XANES spectroscopy to investigate the sulfur oxidation state and speciation in silicate glasses, with sulfur concentrations as low as 450 ppm up to 3000 ppm.[41] In the XANES spectra of some samples only one dominating sulfate peak could be observed, while other samples showed both sulfide and sulfate in their spectra. There was no indication of other sulfur species with intermediate oxidation states between −2 and +6. The shape of the peak at ~2473 eV in the spectrum of the most strongly reduced glass resembled that of pyrrhotite ($Fe_{1-x}S$).

## 6 Future developments

The development of dedicated beamlines for sulfur XANES spectroscopy has opened up numerous fields of application exploring the new possibilities. The initial analyses and speciation of sulfur compounds in low concentrations, down to a few 100 ppm in natural samples and complex mixtures, enabled new insight into environmental and biochemical processes. The emerging detailed theoretical interpretation of both L- and K-edge sulfur XANES spectroscopy will allow further understanding of vital life science processes by the detailed insight possible into the connection between electronic structure and chemical bonding in sulfur compounds, as the studies by Solomon *et al.* already have shown.[11] Development of easy to handle, yet sufficiently accurate, theoretical methods of interpretation is in progress.[42] A great advantage for such studies, *e.g.* of metalloenzymes, is that the X-ray absorption probe can also be tuned to the metal atoms, to achieve structural information also, by EXAFS studies.

 

Scanning X-ray microspectroscopy allows detailed images of the distribution of different sulfur compounds by scanning a sample area at resonance energies of sulfur compounds at the K-edge, with high energy resolution (<0.5 eV) and spatial resolution (<1 μm). Combinations with scanned images of *e.g.* iron distributions or FT-IR vibrational information on the same sample at a beamline (recently available *e.g.* at ID21, ESRF), has allowed detailed conclusions on how hydrogen sulfide enters, reacts and accumulates as solid sulfur compounds in water-logged wood, an important pathway in the sulfur cycle.[38,39] The development of powerful microprobes with even higher resolution is in progress at several synchrotron facilities and will provide a new dimension of information in environmental and life science studies. By covering the samples with a thin film (~4 μm) of sulfur-free polypropylene, wet samples and solutions can also be measured at the K-edge. Current instrumental developments will also allow sulfur L-edge measurements on moist surfaces which is often the case for environmental samples. Ultra high vacuum pumping can keep the detectors in vacuum conditions while a cryogenic pumping system still permits a high pressure environment close to the surface of the samples.

## Acknowledgements

This review article is the outcome of many stimulating discussions over the years with my mentors in X-ray absorption spectroscopy Professor Magnus Sandström (Stockholm University, Sweden), Professor Britt Hedman and Dr Patrick Frank (Stanford University, US), for which I am truly grateful. Special thanks are due to Professor Keith O. Hodgson (Stanford University, US) for providing me with the opportunity to learn this technique, while being Research Associate in his group. Authentic sulfur K-edge XANES spectra of the $Fe_4S_4$ cluster, FeS, L-cysteine, L-cystine, L-methionine, methionine sulfoxide, L-cysteine sulfinic acid, mesylic acid, $SO_4^{2-}$ and $HSO_4^-$ solutions, elemental sulfur ($S_8$ solid) and *myo*-inositol hexasulfate (Fig. 1, 3 and 7) were kindly supplied by Dr Patrick Frank and Professor Britt Hedman, of the Stanford Synchrotron Radiation Laboratory. Special thanks are due to Dr Masoud Kasrai of the University of Western Ontario, Canada, for providing the sulfur L-edge XANES spectra of the model compounds in Fig. 2.

This work has been financially supported by the Natural Sciences and Engineering Council (NSERC) of Canada and its University Faculty Award (UFA) program, the Canadian Foundation of Innovations (CFI), and the Province of Alberta (ASRIP). The X-ray absorption spectra shown in Fig. 4 and 5 were measured at the Stanford Synchrotron Radiation Laboratory (SSRL proposal No. 2848) and the Photon Factory, Tsukuba, Japan (proposal No. 2003G286), respectively. The SSRL Structural Molecular Biology Program is supported by the Department of Energy, Office of Biological and Environmental Research, and by the National Institutes of Health, National Center for Research Resources, Biomedical Technology Program.

## References

1 P. S. Belton, I. J. Cox and R. K. Harris, *J. Chem. Soc., Faraday Trans. 2*, 1985, **81**, 63–75.
2 R. A. Aitken, S. Arumugam, S. T. E. Mesher and F. G. Riddell, *J. Chem. Soc., Perkin Trans. 2*, 2002, 225–226.
3 J. H. Hubbell and S. M. Seltzer, *Tables of X-ray mass attenuation coefficients and mass energy-absorption coefficients*, National Institute of Standards and Technology, Gaithersburg, MD, 2004, ver. 1.4, ch. 2, [online], available: http://physics.nist.gov/xaamdi.
4 J. Stöhr, *NEXAFS spectroscopy*, Springer, Berlin, 1992, ch. 2, pp. 13–15; ch. 5, pp. 114–137.
5 A. Thompson, I. Lindau, D. Attwood, P. Pianetta, E. Gullikson, A. Robinson, M. Howells, J. Scofield, K. Kim, J. Underwood, J. Kirz, D. Vaughan, J. Kortright, G. Williams and H. Winick, *X-ray data booklet*, Lawrence Berkeley National Laboratory, University of California, Berkeley, CA, 2001, [online], available: http://xdb.lbl.gov.
6 B. Hedman, P. Frank, J. E. Penner-Hahn, A. L. Roe, K. O. Hodgson, R. M. K. Carlson, G. Brown, J. Cerino, R. Hettel, T. Troxel, H. Winick and J. Yang, *Nucl. Instrum. Methods Phys. Res., Sect. A*, 1986, **246**, 797–800.
7 E. I. Solomon and M. A. Hanson, in *Inorganic electronic structure and spectroscopy*, ed. E. I. Solomon and A. B. P. Lever, John Wiley & Sons, New York, 1999, vol. II, ch. 1, p. 106.
8 H. H. Zhang, B. Hedman and K. O. Hodgson, in *Inorganic electronic structure and spectroscopy*, ed. E. I. Solomon and A. B. P. Lever, John Wiley & Sons, New York, 1999, vol. I, ch. 9, p. 513–517.
9 G. N. George and M. L. Gorbaty, *J. Am. Chem. Soc.*, 1989, **111**, 3182–3186.
10 G. P. Huffman, S. Mitra, F. E. Huggins, N. Shah, S. Vaida and F. Lu, *Energy Fuels*, 1991, **5**, 574–581.
11 E. I. Solomon, B. Hedman, K. O. Hodgson, A. Dey and R. K. Szilagyi, *Coord. Chem. Rev.*, 2005, **249**, 97–129.
12 P. Frank, B. Hedman and K. O. Hodgson, *Inorg. Chem.*, 1999, **38**, 260–270.
13 A. Vairavamurthy, *Spectrochim. Acta, Part A*, 1998, **54**, 2009–2017.
14 G. Sarret, J. Connan, M. Kasrai, G. M. Bancroft, A. Charri'e-Duhaut, S. Lemoine, P. Adam, P. Albrecht and L. Eybert-B'erard, *Geochim. Cosmochim. Acta*, 1999, **63**, 3767–3779.
15 E. Hudson, D. A. Shirley, M. Domke, G. Remmers, A. Puschmann, T. Mandel, C. Xue and G. Kaindl, *Phys. Rev. A*, 1993, **47**, 361–373.
16 E. Y. Yu, I. J. Pickering, G. N. George and R. C. Prince, *Biochim. Biophys. Acta*, 2001, **1527**, 156–160.
17 B. Hedman, P. Frank, S. F. Gheller, A. L. Roe, W. E. Newton and K. O. Hodgson, *J. Am. Chem. Soc.*, 1988, **110**, 3798–3805.
18 A. Vairavamurthy, W. Zhou, T. Eglinton and B. Manowitz, *Geochim. Cosmochim. Acta*, 1994, **58**, 4681–4687.
19 H. Sekiyama, N. Kosugi, H. Kuroda and T. Ohta, *Bull. Chem. Soc. Jpn.*, 1986, **59**, 575–579.
20 K. R. Williams, B. Hedman, K. O. Hodgson and E. I. Solomon, *Inorg. Chim. Acta*, 1997, **263**, 315–321.
21 M. Kasrai, J. R. Brown, G. M. Bancroft, Z. Yin and K. H. Tan, *Int. J. Coal Geol.*, 1996, **32**, 107–135.
22 D. Attwood, *Soft X-rays and extreme ultraviolet radiation: principles and applications*, Cambridge University Press, Cambridge, UK, 2000, ch. 1, pp. 1–10.
23 M. Kasrai, G. M. Bancroft, R. W. Brunner, R. G. Jonasson, J. R. Brown, K. H. Tan and X. Feng, *Geochim. Cosmochim. Acta*, 1994, **58**, 2865–2872.
24 I. J. Pickering, R. C. Prince, T. Divers and G. N. George, *FEBS Lett.*, 1998, **441**, 11–14.
25 I. J. Pickering, G. N. George, E. Y. Yu, D. C. Brune, C. Tuschak, J. Overmann, J. T. Beatty and R. C. Prince, *Biochemistry*, 2001, **40**, 8138–8145.
26 G. N. George, S. J. George and I. J. Pickering, *EXAFSPAK*; Stanford Synchrotron Radiation Laboratory (SSRL), Menlo Park, CA, 2001, available at: http://www-ssrl.slac.stanford.edu/exafspak.html.
27 B. Leung, F. Jalilehvand and R. Szilagyi, unpublished work.
28 T. Glaser, B. Hedman, K. O. Hodgson and E. I. Solomon, *Acc. Chem. Res.*, 2000, **33**, 859–868.
29 J. Majzlan and S. C. B. Myneni, *Environ. Sci. Technol.*, 2005, **39**, 188–194.
30 A. Dey, N. Ueyama, T. Okamura, B. Hedman, K. O. Hodgson and E. I. Solomon, *J. Am. Chem. Soc.*, 2005, **127**, 12046–12053.

31 E. Damian, F. Jalilehvand, A. Abbasi, L. G. M. Pettersson and M. Sandström, *Phys. Scr., T*, 2005, **115**, 1077–1079.
32 A. Rompel, R. M. Cinco, M. J. Latimer, A. E. McDermott, R. D. Guiles, A. Quintanilha, R. M. Krauss, K. Sauer, V. K. Yachandra and M. P. Klein, *Proc. Natl. Acad. Sci. U. S. A.*, 1998, **95**, 6122–6127.
33 A. Prange, I. Arzberger, C. Engemann, H. Modrow, O. Scumann, H. G. Trüper, R. Steudel, C. Dahl and J. Hormes, *Biochim. Biophys. Acta*, 1999, **1428**, 446–454.
34 E. Y. Sneeden, H. H. Harris, I. J. Pickering, R. C. Prince, S. Johnson, X. Li, E. Block and G. N. George, *J. Am. Chem. Soc.*, 2004, **126**, 458–459.
35 A. Schmidt and K. Jager, *Annu. Rev. Plant Physiol. Plant Mol. Biol.*, 1992, **43**, 325–349.
36 F. Jalilehvand, in *Sulfur transport and assimilation in plants in the post genomic era*, ed. K. Saito, L. J. De Kok, I. Stulen, M. J. Hawkesford, E. Schnug, A. Sirko and H. Rennenberg, Backhuys Publishers, Leiden, Netherlands, 2005, pp. 53–57.
37 M. Sandström, F. Jalilehvand, I. Persson, U. Gelius, P. Frank and I. Hall-Roth, *Nature*, 2002, **415**, 893–897.
38 M. Sandström, F. Jalilehvand, E. Damian, Y. Fors, U. Gelius, M. Jones and M. Salomé, *Proc. Natl. Acad. Sci. U. S. A.*, 2005, **102**, 14165–14170.
39 Y. Fors and M. Sandström, *Chem. Soc. Rev.*, 2006, **35**(5), 399.
40 A. Vairavamurthy, D. Maletic, S. Wang, B. Manowitz, T. Eglinton and T. Lyons, *Energy Fuels*, 1997, **11**, 546–553.
41 E. Paris, G. Giuli, M. R. Carroll and I. Davoli, *Can. Mineral.*, 2001, **39**, 331–339.
42 J. J. Rehr and A. L. Ankudinov, *Coord. Chem. Rev.*, 2005, **249**, 131–140.



 